The International Journal of Applied Economics and Econometrics
Vol. 1 No 1 (June 2024); pp 1-17

Reassessment of the Subpolar Gyre's Predictive Power

Erhard Reschenhofer
Department of Statistics and Operations Research
University of Vienna,
e-mail: erhard.reschenhofer@univie.ac.at

Abstract

This paper identifies two conspicuous regions in the North Atlantic by clustering, These regions show strongly above-average and strongly below-average warming, respectively, and might therefore be useful for the monitoring of changes in the strength of the AMOC. The first region, which lies in the north of the subpolar gyre, has so far defied global warming. However, the results of a seasonal analysis indicate a recent rise in temperature in the months from July to October. If this upward trend continues, it will mask the large AMO fluctuations, which contribute significantly to the variance and auto-correlation of northern temperature time series. The common use of increases in these second moments as early-warning signs for an imminent AMOC collapse will then be deprived of its basis. Moreover, empirical evidence suggests that past increases were erratic and not steady, which makes it fundamentally impossible to predict the time of a possible AMOC collapse by extrapolation.

Keywords: Global warming, AMOC collapse, early-warning signs, variance, autocorrelation.

1. Introduction

The circulation in the North Atlantic is caused by differences in temperature and salinity. The Gulf Stream, which is a part of this circulation, transports a large amount of heat from the south to the north. A weakening of the Gulf Stream might therefore entail a cooling in the north and a warming in the south or, in the presence of global warming, an accelerated warming in the south and a delayed warming in the north. Carrying out simulations with a global climate model, Latif et al. (2004) indeed found a relationship in the low-frequency range between the North Atlantic thermohaline circulation and the sea surface temperature (SST) in a specific northern region (40°–60°N and 50°–10°W; see the dotted region in Figure 1). Therefore, they proposed a simple method to monitor future changes in this circulation, which consists of just observing sea surface temperatures in that particular region or (because of global warming) rather temperature differences between more northern and more southern regions. Fittingly, Rahmstorf et al. (2015) defined a proxy for the Atlantic Meridional Overturning Current (AMOC) as the difference between the mean temperature in a certain northern region, which they called "subpolar gyre" and which contains the 17 grid points represented by circles with black borders in Figure 1, and the Northern Hemisphere mean surface temperature. The significance of such a proxy stems from the fact that direct measurements of the AMOC are only available for relatively short periods (Smeed et al., 2014), which makes it impossible to distinguish between multidecadal oscillations and longer-term trends. With the help of simulations, Caesar et al.

(2018) identified a characteristic SST fingerprint of an AMOC slowdown, which consists of a cooling in the subpolar gyre region and a warming along the US northeast coast and is most pronounced during winter and spring. However, they based their AMOC proxy only on the former region because of too much variability in the latter region. It is defined as the mean SST in the subpolar gyre from November to May minus the global mean SST from November to May.

The subpolar gyre is characterized by a weaker increase in the temperature compared to other regions. In the presence of long cycles with large amplitudes, the widely used linear trend model is unsuitable for the quantification of this increase. It will inevitably confuse a slight increase with a decrease if the series starts at the maximum of a cycle or ends at the minimum of a cycle. The respective study period obviously plays a major role in this context. For example, Latif et al. (2004), Rahmstorf et al. (2015), and Caesar et al. (2018) studied the periods 1870–1998, 1901–2000, and 1870–2016, respectively. In the next section, a more sophisticated investigation will be carried out. Both the long-term trend and various cycles will be taken into account for the identification of clusters with similar temperature trends. The suitability of the cluster classification for the purpose of assessing and forecasting the AMOC strength will be examined in Section 3. The discussion in Section 4 addresses seasonal and bivariate aspects and concludes.

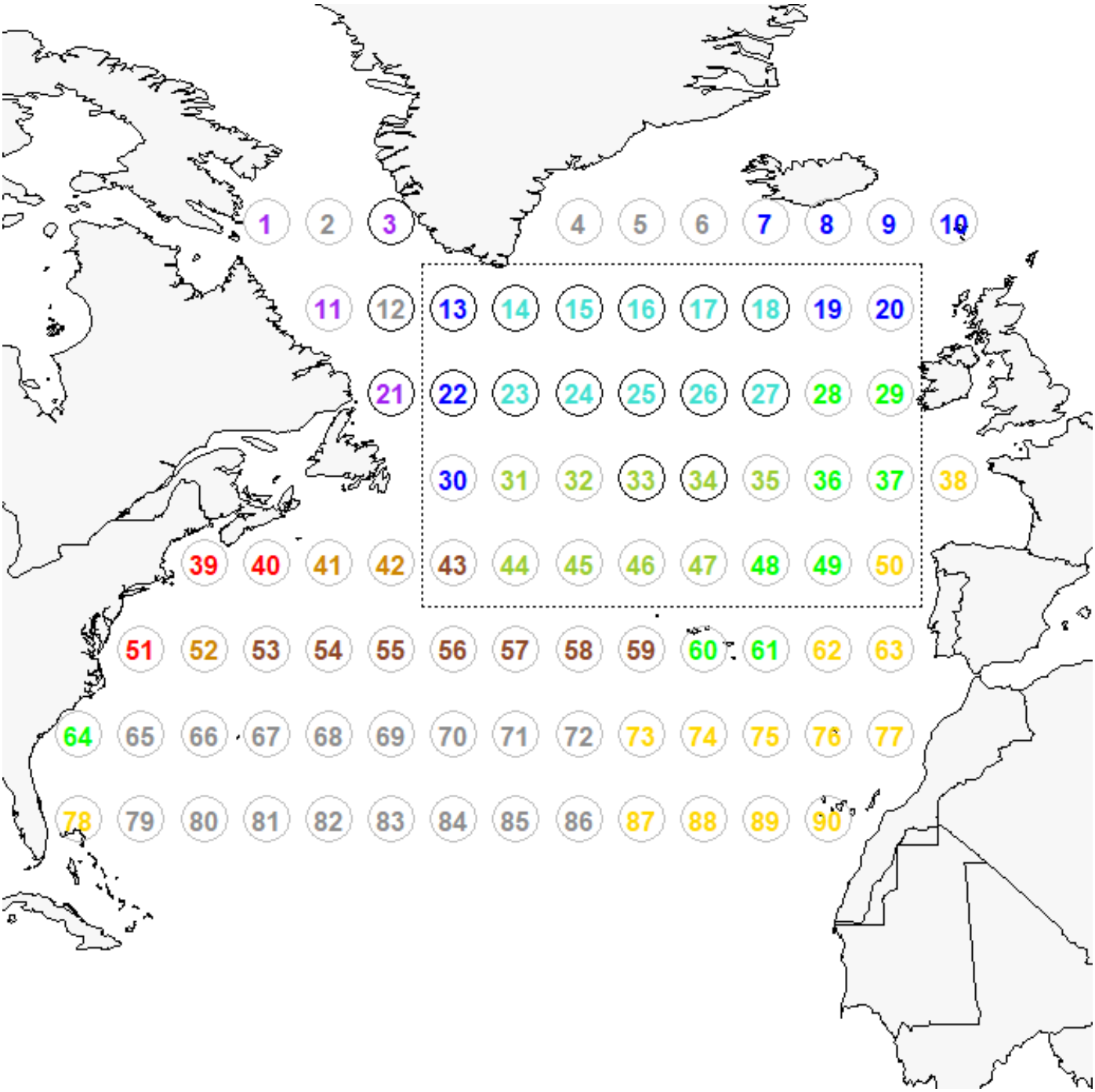

Figure 1: Identification of nine clusters (purple, blue, turquoise, green, yellow green, yellow, red, orange, brown) of grid points with similar temperature trends. The gray points do not form an independent cluster. They were left out because of missing values after December 1873.

2. Clustering

For the statistical analysis, I used the free statistical software R (R Core Team, 2022) and the global land and ocean dataset HadCRUT5 Analysis (from https://crudata.uea.ac.uk/cru/data/temperature/), which combines land [CRUTEM5] and marine [HadSST4] temperature anomalies on a 5° by 5° grid with greater geographical coverage via statistical infilling (Morice et al., 2021). This dataset has been developed by the Climatic Research Unit (University of East Anglia and NCAS) jointly with the Hadley Centre (UK Met Office). The temperatures are expressed as anomalies from the base period 1961-1990. The average temperature for each calendar month in the base period is regarded as normal. The complete series of anomalies are shown for all 90 grid points in Figure 2.

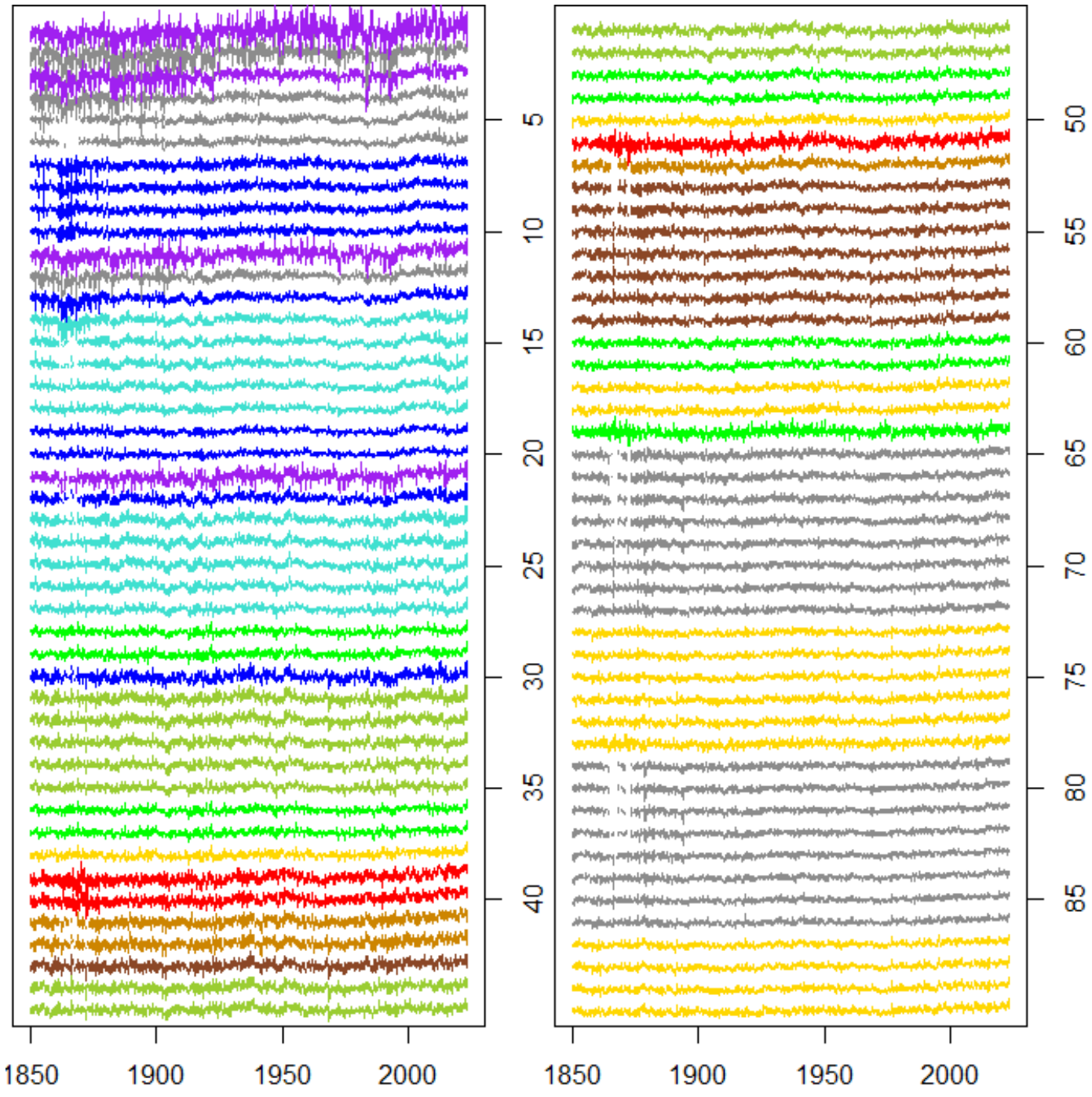

Figure 2: Individual series of anomalies at grid points 1-45 in the first column and 46-90 in the second column. Colors indicate cluster affiliations. The gray series have missing values after December 1873.

The nine clusters of grid points shown in Figure 1 were obtained by first smoothing the individual series of anomalies from January 1874 to July 2023 with the help of the Hodrick-Prescott (HP) filter (using the R function hpfilter of the package mFilter) and then performing k-means clustering on the smoothed series (choosing the Hartigan–Wong algorithm for the R function kmeans). The HP trend F_t of the series $X_1, \ldots, X_n$ is obtained by minimization of

$$\sum_{t=1}^{n}(X_t - F_t)^2 + \Lambda \sum_{t=3}^{n}((F_t - F_{t-1}) - (F_{t-1} - F_{t-2}))^2, \quad (1)$$

where the tuning parameter Λ determines the degree of smoothing. For the series of anomalies, the value $\Lambda = 10^7$ was used. For each cluster, the individual HP trends are shown in Figure 3. Obviously, the agreement within a cluster is very strong. The smooth lines shown in Figure 4 represent clusterwise averages.

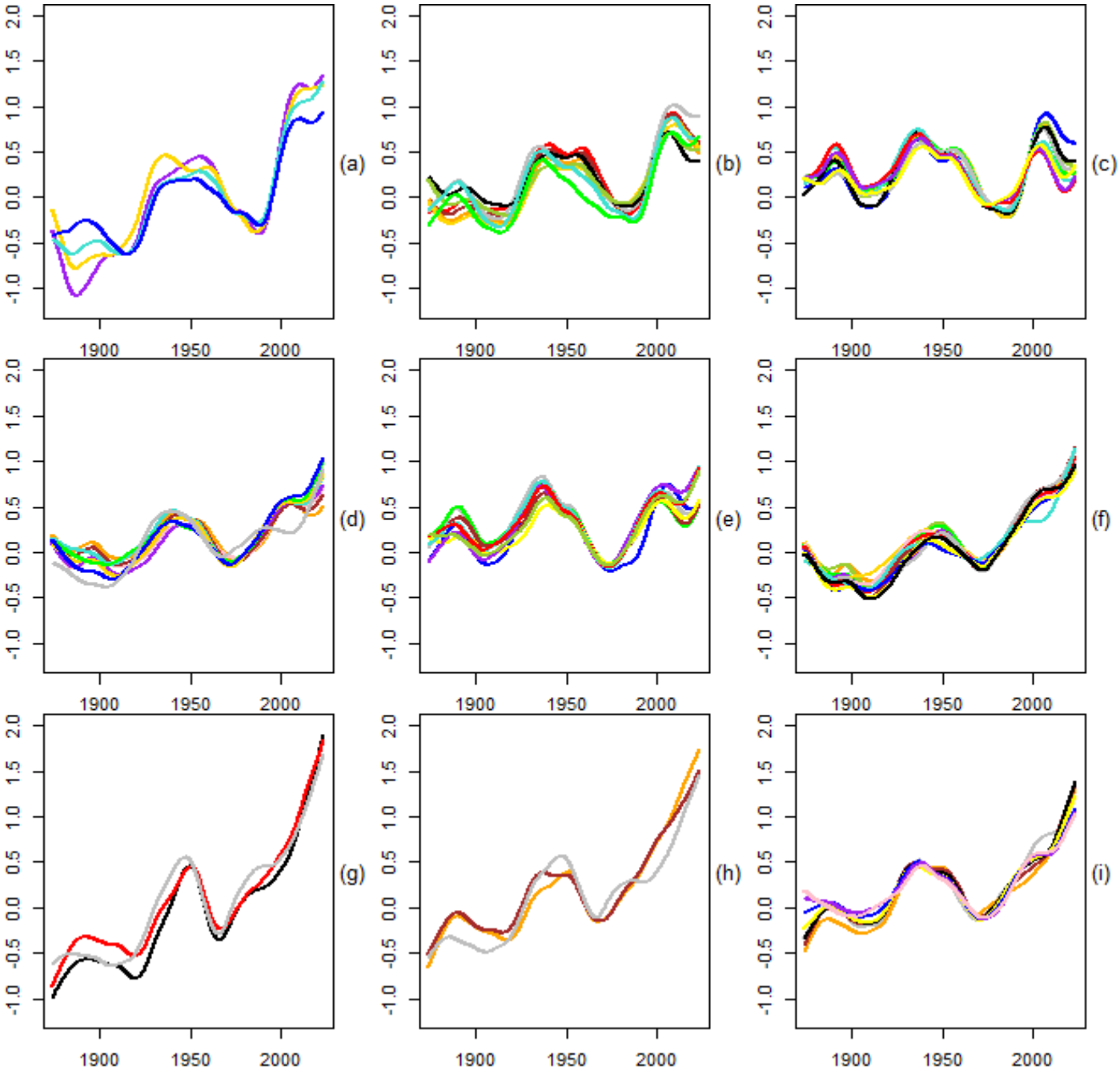

Figure 3: Polynomial temperature trends for each grid point grouped by clusters (a: purple cluster, b: blue cluster, c: turquoise cluster, d: green cluster, e: yellow green cluster, f: yellow cluster, g: red cluster, h: orange cluster, i: brown cluster)

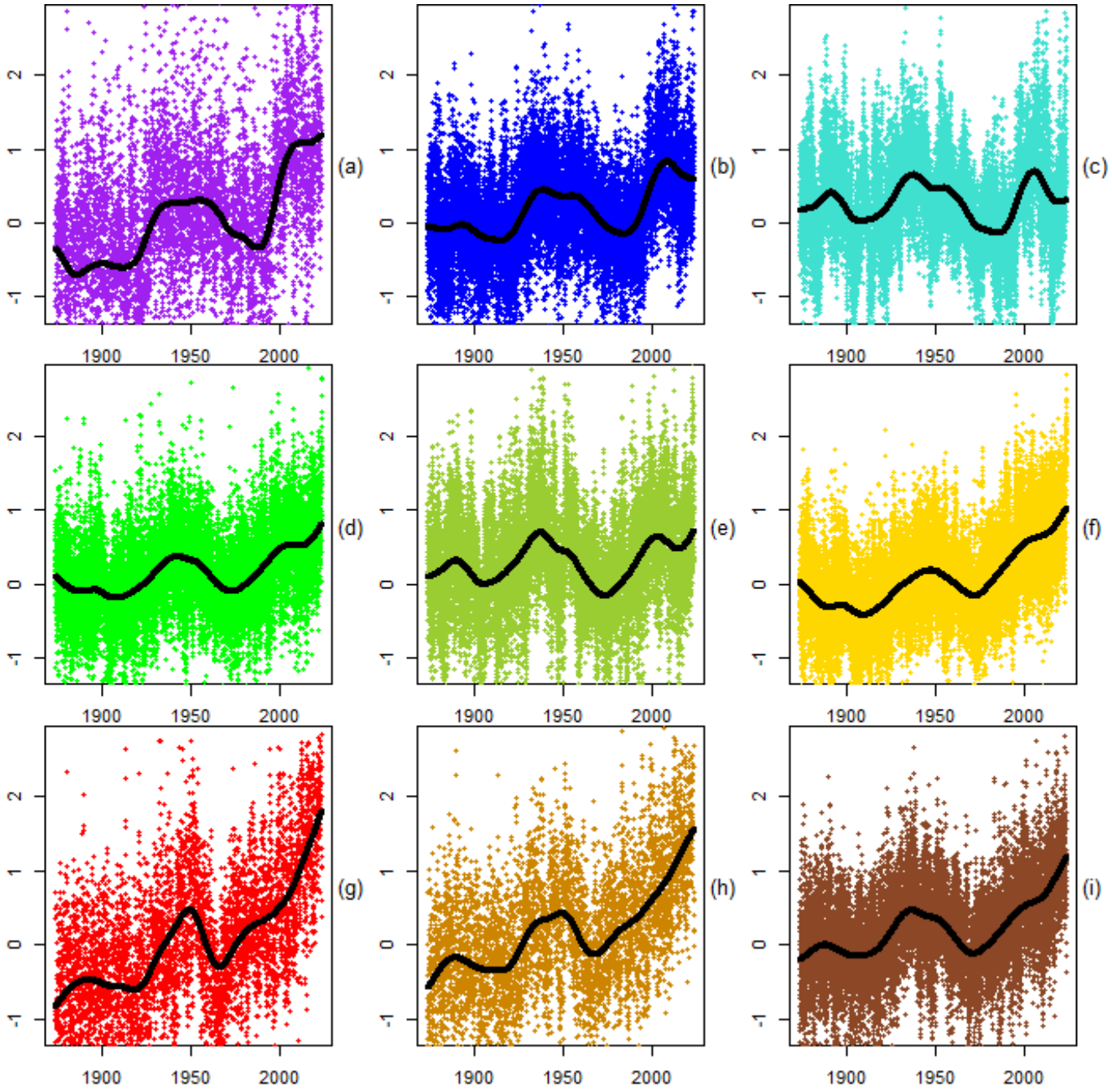

Figure 4: Clusterwise temperature trends (a: purple cluster, b: blue cluster, c: turquoise cluster, d: green cluster, e: yellow green cluster, f: yellow cluster, g: red cluster, h: orange cluster, i: brown cluster)

The small red cluster (with only three grid points) along the US northeast coast and the larger turquoise cluster (with ten grid points) below Greenland show strongly above-average and strongly below-average warming, respectively, and are therefore the natural candidates to indicate a weakening of the AMOC. The next best candidates are the yellow green cluster and the orange cluster, respectively.

3. Early-warning signs

As mentioned earlier, the difference between the mean temperature in the subpolar gyre, which contains the turquoise cluster as a subset, and some global or hemispheric benchmark has already been

proposed as a proxy for the AMOC strength. The Northern Hemisphere mean surface temperature was used as benchmark by Rahmstorf et al. (2015), the global mean SST by Caesar et al. (2018), and two times the global mean SST by Ditlevsen and Ditlevsen (2023). The factor 2 in the last benchmark was justified by polar amplification (see Holland and Bitz, 2003). Using several SST-based and salinity-based AMOC proxies, Boers (2021) found early-warning signs, such as increasing variance and autocorrelation, that the AMOC could be close to a critical transition to a weaker circulation mode. Ditlevsen & Ditlevsen (2023) went even further and extrapolated the sample autocorrelation of their detrended proxy in order to determine when this critical transition will happen. However, Reschenhofer (2023) questioned the reliability of a forecast made in this way because of its critical dependence on the adequacy of the underlying statistical model, the plausibility of certain assumptions, the quality of the involved approximations, the arbitrary choice of the AMOC proxy, the method of trend estimation, the size of the rolling window used for the estimation of the second moments, the determination of the start time of ramping, etc. Changing only a single specification was enough to move the predicted time of the AMOC collapse by several decades. Perhaps the most serious point of criticism was that the autocorrelation appears to increase erratically rather than steadily which would make forecasting based on extrapolation impossible.

Before we can estimate the variance and the autocorrelation, we must first look at the trend. In the first three of its columns, Figure 5 shows a kind of trend decomposition separately for each cluster. The HP trend $F_t^{(1)}$ for the cluster means X_t (with $\Lambda = 2.5 \cdot 10^9$) is the first component, the HP trend $F_t^{(2)}$ for the deviations $D_t = X_t - F_t^{(1)}$ (with $\Lambda = 2.5 \cdot 10^7$) is the second component, and the HP trend $F_t^{(3)}$ for the deviations $V_t = D_t - F_t^{(2)}$ (with $\Lambda = 2.5 \cdot 10^6$) is the third component. However, only the first component could possibly be interpreted as a trend in the strict statistical sense. The second corresponds rather to an oscillation with large but varying amplitudes and long but varying periods (such as the Atlantic Multidecadal Oscillation) and appears as a peak at the second Fourier frequency in the periodogram of the detrended series D_t (see the last column of Figure 5). The third also looks like a fairly regular oscillation and appears as a somewhat smaller peak at the 7th Fourier frequency.

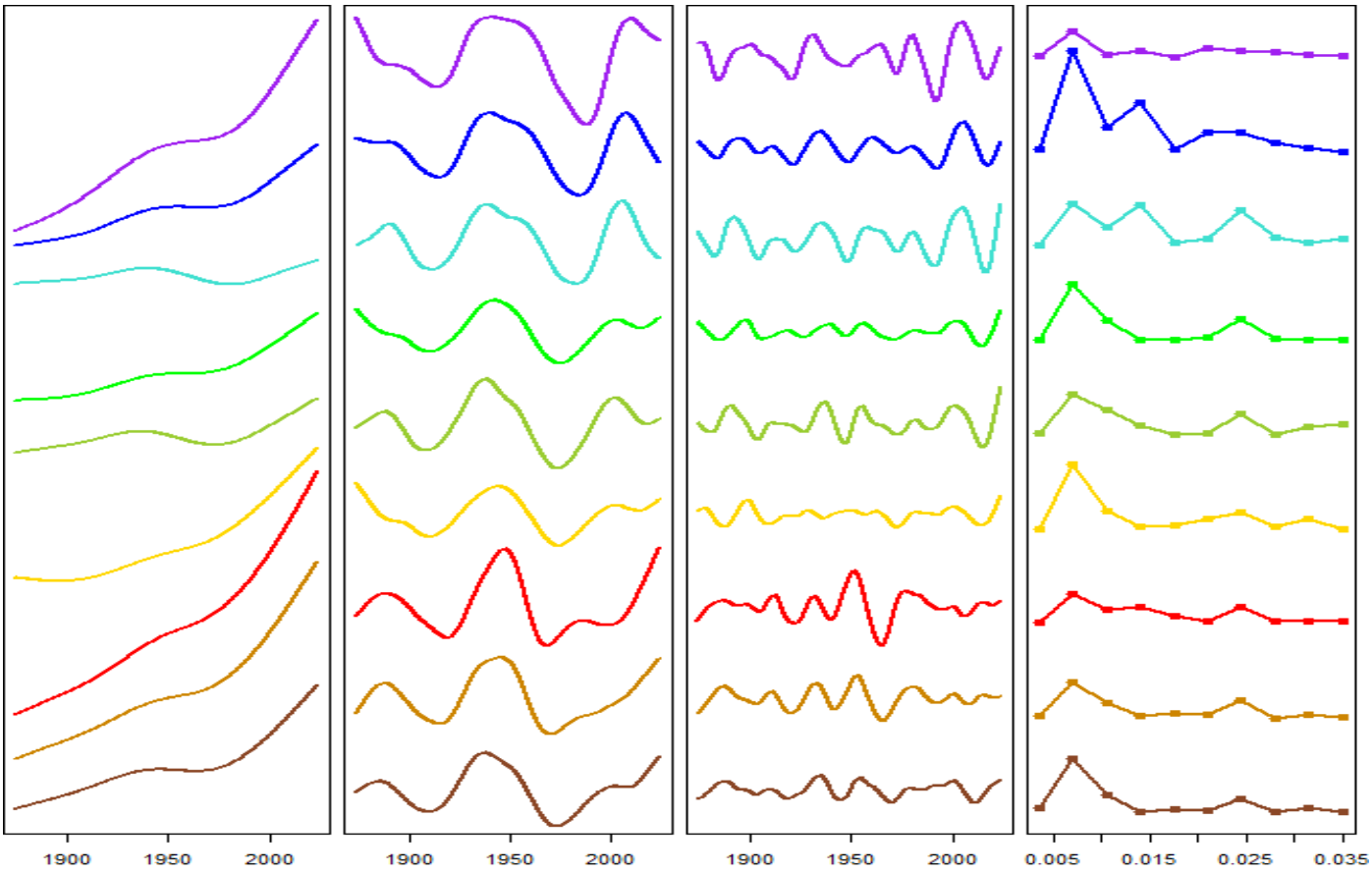

Figure 5: Clusterwise long-term temperature trends (first column), lower-frequency oscillations (second column), higher-frequency oscillations (third column) and first ten periodogram ordinates of detrended temperature series (fourth column)

For a more in-depth analysis, the four most conspicuous clusters (turquoise, yellow green, red, and orange) were selected first. Then, for each of these clusters, the HP trend with $\Lambda = 2.5 \cdot 10^9$ was obtained from the cluster means and the trend residuals U_t were calculated. Finally, the statistics U_t^2/n and $R_t/(n-1)$, where

$$R_t = \frac{\pi}{\pi-2} sign(U_{t-1}U_t) \frac{\min(|U_{t-1}|,|U_t|)}{\max(|U_{t-1}|,|U_t|)} \quad (2)$$

(see Reschenhofer, 2017a, 2017b, 2019), were plotted cumulatively against time. The advantage of this approach is that changes in the variance and the first-order autocorrelation can be detected without any delay caused by an estimation window. In contrast, windows of width 50 and 70 years were used by Ditlevsen and Ditlevsen (2023) and Boers (2021), respectively. The bias of the autocorrelation estimator R_t does not really bother as long as only changes in the autocorrelation are of interest. There are no indications of a steadily growing variance or autocorrelation in the second and fourth column of Figure 6. An occasional change in the slope of a cumulative plot is certainly not suspicious and can in any case be better explained by a structural break.

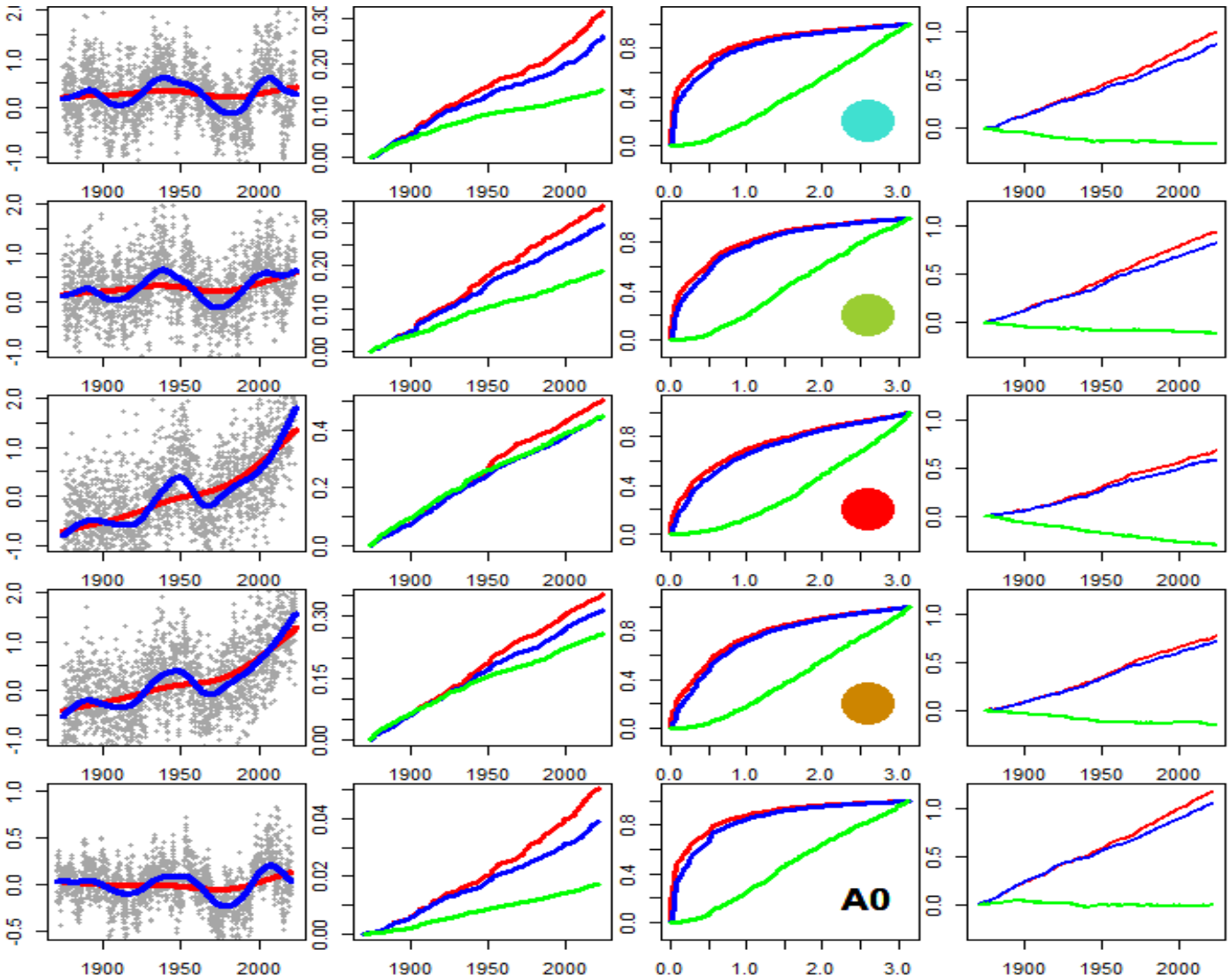

Figure 6: For the turquoise, yellow green, red, and orange cluster as well as for the subpolar gyre, two HP trends are shown in the first column, the cumulative squared trend residuals in the second column, the normalized cumulative periodogram of the residuals in the third column, and a cumulative upward-biased measure of autocorrelation in the fourth column. The green lines were obtained by replacing the trend residuals by first differences.

Not surprisingly, choosing a much smaller value of the smoothing parameter Λ (such as $\Lambda = 2.5 \cdot 10^7$), which fails to remove the multidecadal oscillations from the trend, yields both a smaller variance and a smaller autocorrelation (see Figure 6). Differencing is an alternative way to get rid of the trend. However, this transformation will usually turn a positive autocorrelation into a negative one. Moreover, we may expect that the autocorrelation of the differenced series vanishes as the autocorrelation of the original series approaches 1. The cumulative plots created for the first differences bring no surprises. Also, their normalized cumulative periodograms do not exhibit any features of interest. They are largely linear apart from a power deficiency near frequency zero which is due to differencing. In contrast, the normalized cumulative periodograms of the trend residuals indicate a peak at frequency zero, which also was to be expected in view of the presence of long cycles.

Not much changes when the same analysis is carried out again after subtracting two times the global mean SST from the cluster means (see Figure 7). There is still no clear indication of a steady

increase in variance or autocorrelation, which is also in line with the results obtained with the time series A0 (subpolar gyre) and A2 (AMOC proxy) that were kindly provided by Ditlevsen and Ditlevsen (2023) online in a repository (see the last rows of Figures 6 and 7, respectively).

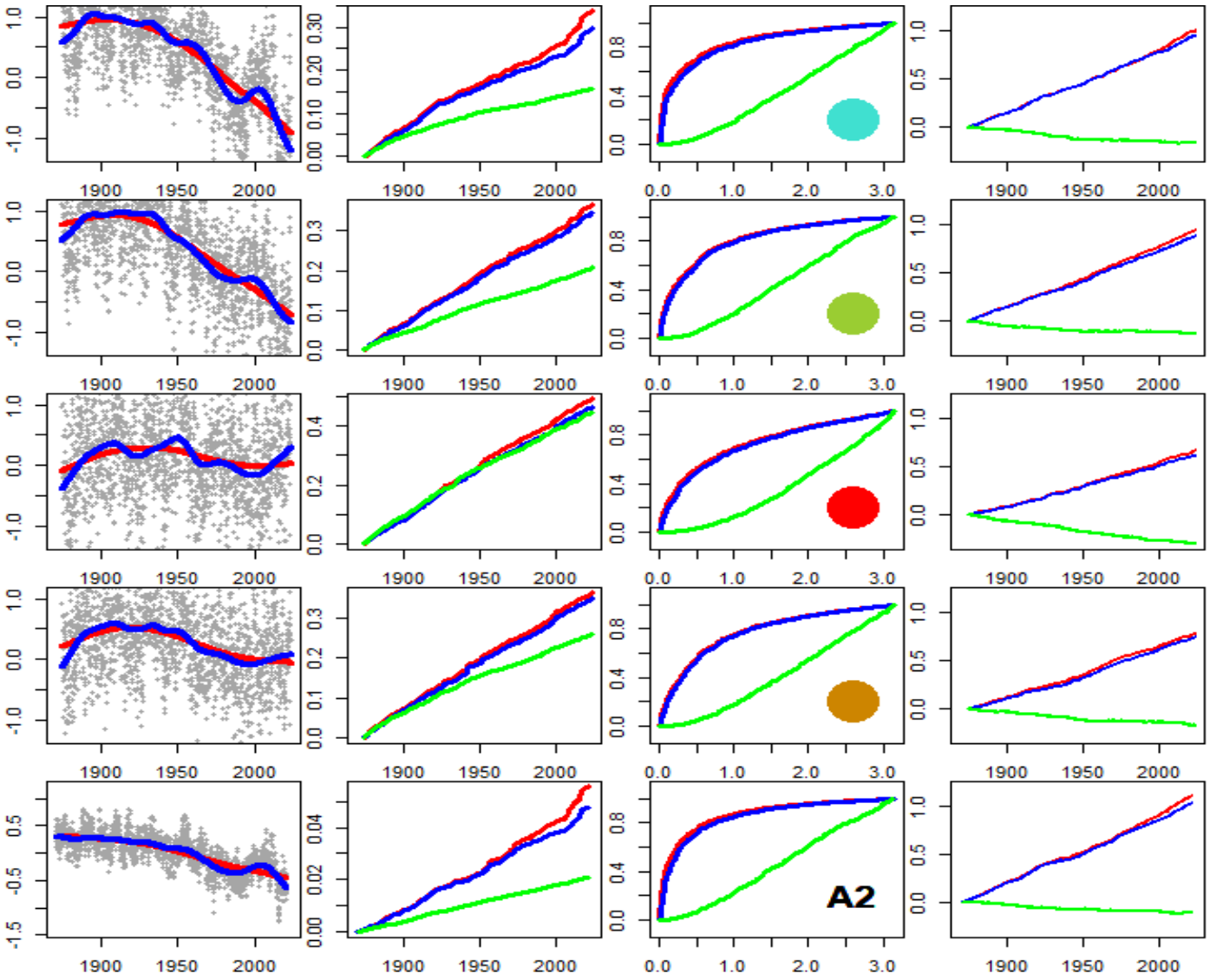

Figure 7: For each AMOC proxy based on the turquoise, yellow green, red, and orange cluster as well as on the subpolar gyre, respectively, two HP trends are shown in the first column, the cumulative squared trend residuals in the second column, the normalized cumulative periodogram of the trend residuals in the third column, and a cumulative upward-biased measure of autocorrelation in the fourth column. The green lines were obtained by replacing the trend residuals by first differences.

The contribution of the Atlantic Multidecadal Oscillation (AMO) to the variance and the autocorrelation is illustrated in Figure 8. The anomalies of the turquoise cluster are shown together with two fitted HP trends obtained with $\Lambda = 2.5 \cdot 10^9$ and $\Lambda = 10^7$, respectively. The first represents the long-term trend and the second represents the AMO. In the northern part of the cluster (first column of Figure 8), the amplitude of the last complete AMO cycle (with a minimum slightly before 1990 and a maximum slightly after 2000) is strikingly large. There is a big bunch of values far below the trend line followed by another big bunch of values far above the trend line, which provide exactly the right conditions for both a high variance and a high autocorrelation in that period. However, it seems that the

next AMO minimum will be just below the trend line, which does not leave much room for a further increase in variance and autocorrelation in the near future. Moreover, the small size of the last bunch of values below the trend line and the sharp temperature rise at the very end of the observation period (particularly in the southern part of the cluster) suggest that global warming is finally also catching up with the subpolar gyre. Rising temperatures have already masked the AMO in more southern clusters decades ago (see Figure 4.g,h,i).

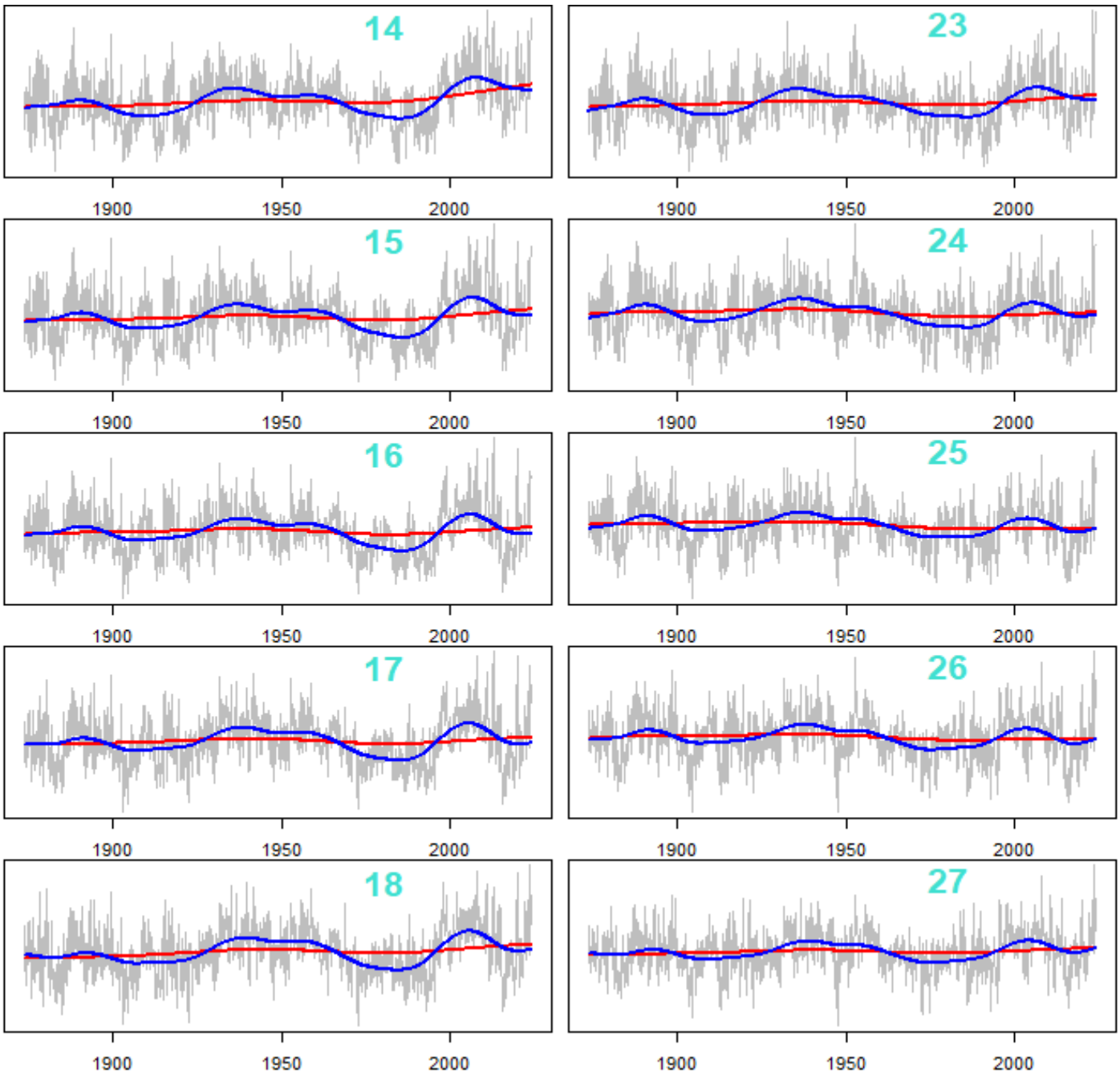

Figure 8: Anomalies of the turquoise cluster together with two fitted HP trends

Figures 6 and 7 only give a rough impression of the change in variance and autocorrelation. Focusing on a single grid point brings out more details. For the grid point in the middle of the northern part of the turquoise cluster, Figure 9 shows the cumulative squared trend residuals and the cumulative squared first differences as well as cumulative measures of autocorrelation both for the trend residuals

and the first differences. In addition to the statistic (2), which is based on only two observations, Burg's estimator

$$\tilde{\rho}(k) = \frac{2\sum_{s=t-k+1}^{t} U_s U_{s-1}}{\sum_{s=t-k}^{t-1} U_t^2 + \sum_{t=t-k+1}^{t} U_t^2} \tag{3}$$

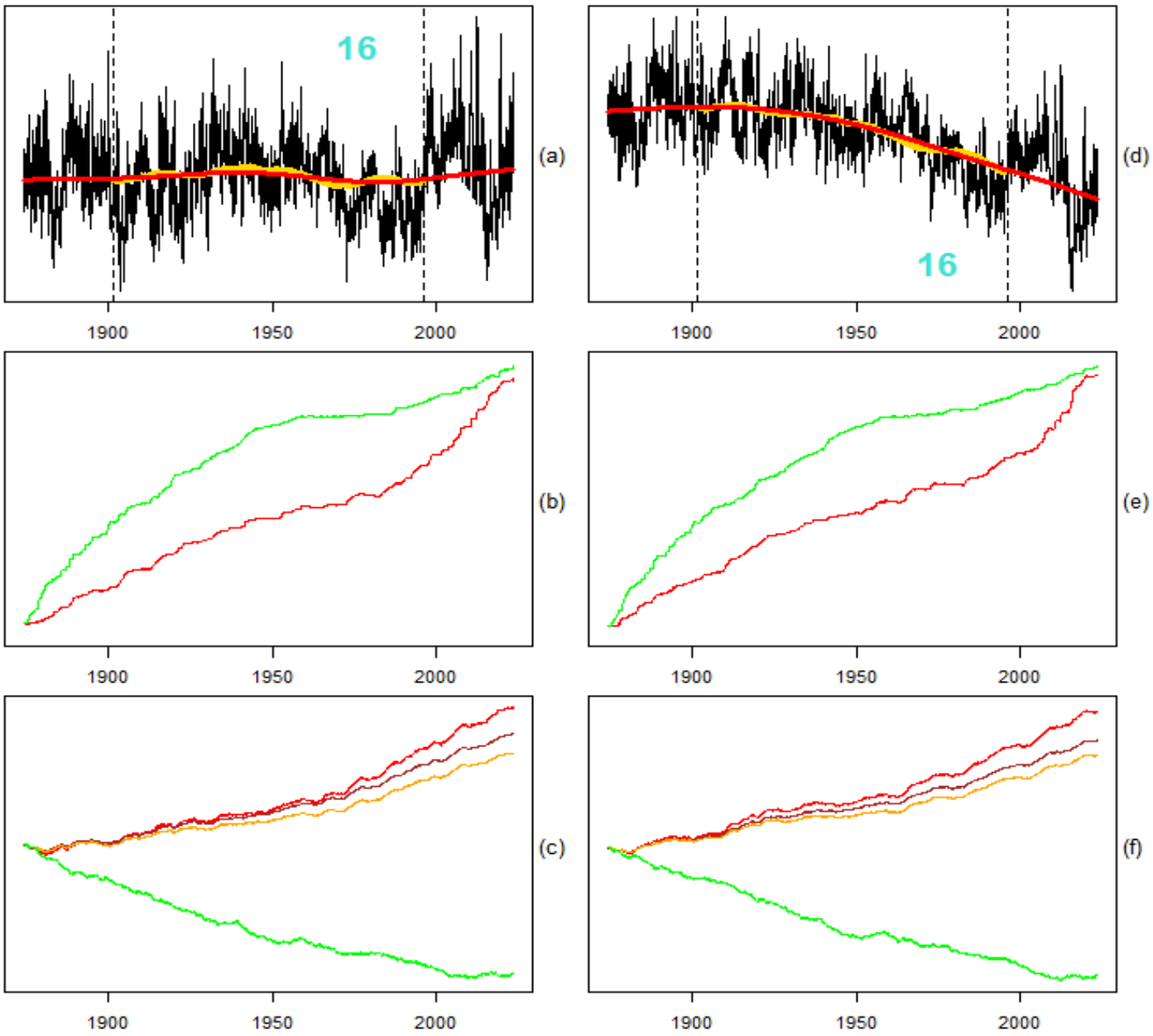

Figure 9: First row: Anomalies at grid point 16 (a: raw, b: minus two times the global mean SST) together with fitted HP trend ($\Lambda = 2.5 \cdot 10^9$: red) and moving averages (window size =55*12+1: yellow)
Second row: Cumulative squared trend residuals (red) and cumulative squared first differences (green)
Third row: Cumulative measures of autocorrelation for the trend residuals (Reschenhofer, 2017a: red, Burg, 1967, 1975 with $k = 2$ and $k = 3$: orange and brown, respectively) and the first differences (Reschenhofer, 2017a: green)
To make it easier to recognize structural breaks, suitable straight lines have been subtracted from the cumulative graphs.

(Burg, 1967, 1975), which is based on k observations, is also included for $k = 2$ and $k = 3$, respectively. Compared to the least squares estimator

$$\hat{\rho}(k) = \frac{\sum_{s=t-k+1}^{t} U_s U_{s-1}}{\sum_{s=t-k}^{t-1} U_t^2}, \tag{4}$$

Burg's estimator has the advantage that it does not take values outside the open interval (−1,1) with positive probability. Although the individual statistics, which are based on a very small number of observations, are extremely volatile, any noticeable change in the slope of the cumulative graph is a clear indication of a structural break. Overall, there appear to be two breaks in the variance, one around 1950 and the second around 1980, and at least one break in the autocorrelation around 1960. There are no indications of a steadily growing variance or autocorrelation regardless of whether the series of anomalies is used or the AMOC proxy, which is obtained by subtracting two times the global mean SST.

4. Discussion

Unlike other researchers, Caesar et al. (2018) incorporated seasonal aspects into the definition of their AMOC proxy. In order not to overlook anything important, it is therefore advisable to check whether there are any significant differences between the various calendar months. Figure 10 shows the HP trends ($\Lambda = 2.5 \cdot 10^4$) of the cluster means separately for each calendar month. The only really noticeable pattern occurs in the first (purple) cluster during the "winter months" (from December to March). In the more interesting third (turquoise) cluster, there has recently been a slight warming in the "summer months" (from July to October). Using only the period from November to May like Caesar et al. (2018) might therefore indeed emphasize the different nature of this cluster.

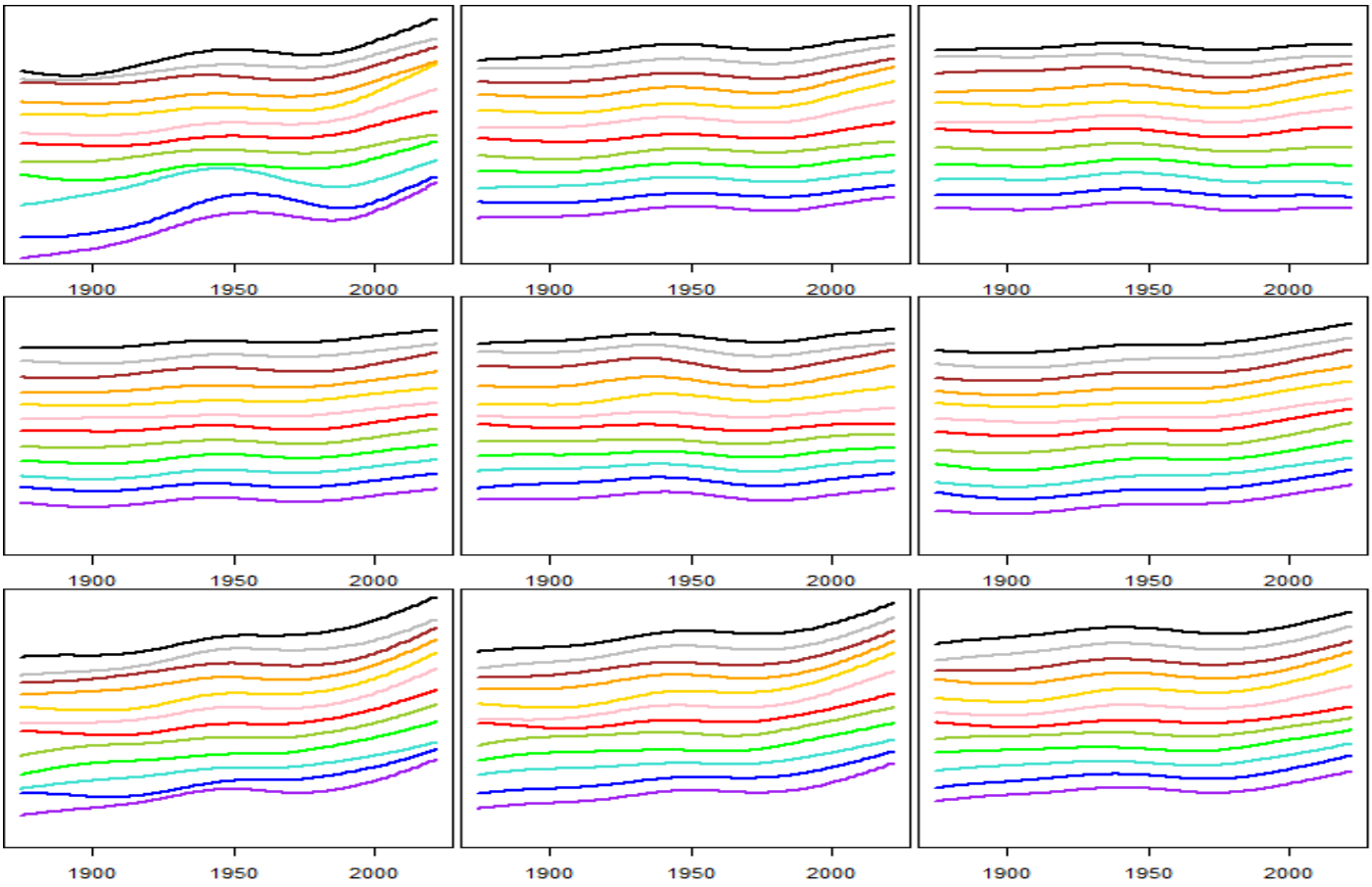

Figure 10: HP trends ($\Lambda = 2.5 \cdot 10^4$) of the cluster means for each calendar month (January: purple, February: blue, March: turquoise, April: green, May: yellow green, June: red, July: pink, August: yellow, September: orange, October: brown, November: gray, December: black)

Defining an AMOC proxy as the difference of two temperature series is, of course, not yet a bivariate analysis. For the sake of completeness, the results of a cross spectral analysis for the clusters 3 (turquoise), 5 (yellow green), 7 (red), 8 (orange) are therefore presented in Figure 11 (for a univariate spectral analysis see, e.g., Mangat and Reschenhofer, 2020). The squared coherencies displayed below the main diagonal show no conspicuous features, possibly apart from a peak near frequency zero in the case of the cluster combination 3 & 5. To avoid artificial jumps (e.g, from π to $-\pi$) caused by the non-uniqueness of the polar coordinates and thereby improve the interpretability of the estimated phase spectra displayed above the main diagonal, two additional versions of the phase spectra obtained by adding and subtracting 2π have also been plotted. However, it seems that none of the four series of cluster means is leading or lagging because the phase spectra are pretty flat, at least in the frequency ranges with higher cross correlation.

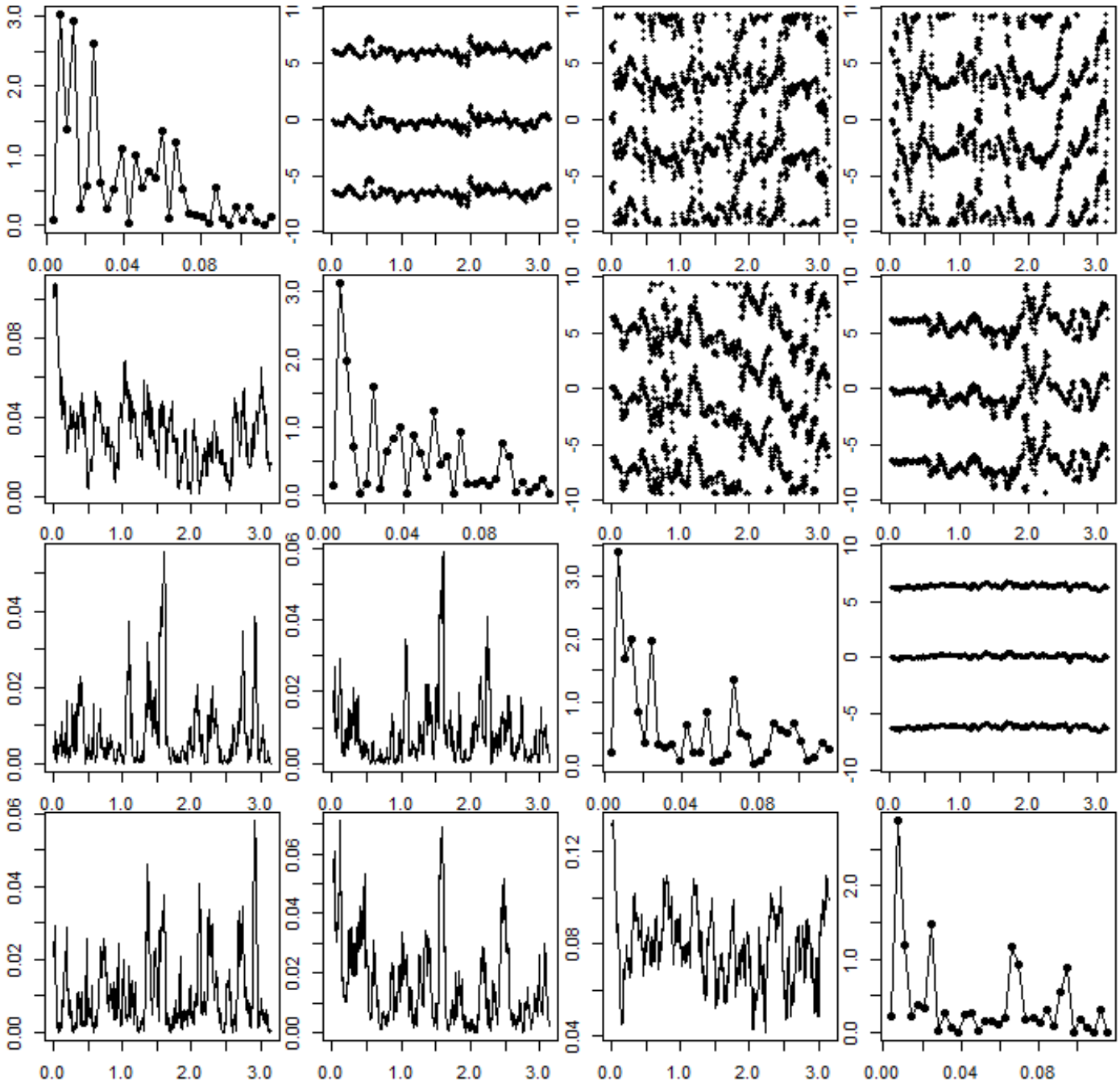

Figure 11: Cross spectral analysis (width of modified Daniell smoother = 25) of the detrended ($\Lambda = 2.5 \cdot 10^9$) cluster means (3: turquoise, 5: yellow green, 7: red, 8: orange)
Main diagonal: periodograms (3, 5, 7, 8)
Above: phase spectra (3 & 5, 3 & 7, 3 & 8, 5 & 7, 5 & 8, 7 & 8), below: squared coherencies

Also, the mere subtraction of a global or hemispheric benchmark from a series of anomalies adds no real value when it comes to the monitoring of early-warning signs for a weakening AMOC. Clearly, the short-term fluctuations of the benchmark are not helpful in this respect. The same is true for the long-term trend of the benchmark, which has to be removed anyway when the variance and autocorrelation are calculated locally. It is therefore not surprising that the first column of Figure 9 (without subtraction) looks very much like the second column (with subtraction). What remains is the observation that a certain region in the North Atlantic appears to defy global warming, but only with the imposition of increasingly severe regional and seasonal restrictions. Once the rise in temperature

can be observed everywhere and the AMO is masked by the upward trend, there is little scope for a further increase in variance and autocorrelation, which renders these early-warning signs obsolete. The sobering conclusion is that it is currently impossible to make any reliable predictions with the available data and methods.

References

Boers, N. (2021). Observation-based early-warning signs for a collapse of the Atlantic Meridional Overturning Circulation, Nature Climate Change, 11, 680–688.

Burg, J.P. (1967). Maximum Entropy Spectral Analysis, Presented at the 37th Annual International Meeting of the Society of Exploration Geophysicists, Oklahoma City, October, 31st, 1967.

Burg, J.P. (1975). Maximum Entropy Spectral Analysis, PhD thesis, Stanford University.

Caesar, L., Rahmstorf, S., Robinson, A., Feulner, G. and Saba, V. (2018). Observed fingerprint of a weakening Atlantic Ocean overturning circulation, Nature, 556, 191–196.

Ditlevsen, P. and Ditlevsen, S. (2023). Warning of a forthcoming collapse of the Atlantic meridional overturning circulation, Nature Communications ,14, 4254.

Holland, M.M. and Bitz, C.M. (2003). Polar amplification of climate change in coupled models. Climate Dynamics, 21, 221–232.

Latif, M., Roeckner, E., Botzet, M., Esch, M., Haak, H., Hagemann, S., Jungclaus, J., Legutke, S., Marsland, S. Mikolajewicz, U. and Mitchell, J. (2004). Reconstructing, Monitoring, and Predicting Multidecadal-Scale Changes in the North Atlantic Thermohaline Circulation with Sea Surface Temperature, Journal of Climate, 17, 1605-1614.

Mangat, M.K. and Reschenhofer, E. (2020). Frequency-domain evidence for climate change. Econometrics 8, 28.

Morice, C.P., Kennedy, J.J., Rayner, N.A., Winn, J.P., Hogan, E., Killick, R.E., Dunn, R.J.H., Osborn, T.J., Jones, P.D. and Simpson, I.R. (2021). An updated assessment of near-surface temperature change from 1850: the HadCRUT5 dataset, Journal of Geophysical Research, 126, e2019JD032361.

R Core Team (2022). R: A language and environment for statistical computing, R Foundation for Statistical Computing, Vienna, Austria.

Rahmstorf, S., Box, J.E., Feulner, G., Mann, M.E., Robinson, A., Rutherford, S. and Schaffernicht, E.J. (2015). Exceptional twentieth-century slowdown in Atlantic Ocean overturning circulation, Nature Climate Change, 5, 475–480.

Reschenhofer, E. (2017a). Using ratios of successive returns for the estimation of serial correlation in return series, Noble International Journal of Economics and Financial Research, 02, 125-130.

Reschenhofer, E. (2017b). Examining the properties of a simple estimator based on transformed Cauchy variables, Journal of Statistics: Advances in Theory and Applications, 18, 45-54.

Reschenhofer, E. (2019). Heteroscedasticity-robust estimation of autocorrelation, Communications in Statistics - Simulation and Computation, 48, 1251–1263.

Reschenhofer, E. (2023). Improved monitoring of early-warning signs of an AMOC collapse, Working paper.

Smeed, D.A., McCarthy, G., Cunningham, S.A., Frajka-Williams, E., Rayner, D., Johns, W.E., Meinen, C.S., Baringer, M.O., Moat, B.I., Duchez, A., and Bryden, H.L. (2014). Observed decline of the Atlantic Meridional Overturning Circulation 2004 to 2012, Ocean Science Discussions, 10.